Porous Carbon Supports Prepared by Ultrasonic Spray Pyrolysis for Direct Methanol Fuel Cell Electrodes

Jin Ho Bang,[†] Kookil Han,[‡] Sara E. Skrabalak,[†] Hasuck Kim,*,[‡] and Kenneth S. Suslick*,[†]

School of Chemical Sciences, University of Illinois at Urbana-Champaign, 600 South Mathews Avenue, Urbana, Illinois 61801, and Department of Chemistry, Seoul National University, Seoul 151-747, South Korea

Received: February 27, 2007; In Final Form: May 2, 2007

Carbon powders composed of porous micrometer-sized spheres were synthesized from simple organic salt precursors using ultrasonic spray pyrolysis (USP). These materials were tested as catalyst supports for a direct methanol fuel cell (DMFC) catalyst and as pore formers in a membrane electrode assembly (MEA). The effect of these materials on unit cell performance was evaluated and compared to traditional Vulcan XC-72 carbon nanoparticle powder. USP provides a simple and facile way to prepare porous carbons with various morphologies and pore sizes. In exploring these new morphologies of carbon, two types of micrometer-sized spherical porous carbons were tested as pore-forming additives for both the anode catalyst (i.e., PtRu/C for methanol oxidation) and the cathode catalyst (i.e., Pt/C for O_2 reduction). The anode catalyst mixture of PtRu/Vulcan and PtRu/PC-I (weight ratio 2:1, 33 wt % PC-I) showed the highest performance improvement and is attributed to the synergic effect of two carbons (PC-I and Vulcan XC-72); the mixture improves the effective mass transport of reactant methanol and products while maintaining a reasonably high conductivity. For the reduction of O_2 at the cathode, the addition of relatively small amounts of carbon microspheres (PC-II) significantly improved the performance of the cathode when they were added to the E-TEK commercial Pt/C catalyst. Even at a relatively slow airflow rate, the maximum power density of the MEA with 1.25 wt % PC-II was maintained without a significant decrease. O_2 is, of course, much less viscous than methanol, and consistent with that, the amount of pore loading required is much less for the cathode than for the anode (i.e., 1.25 wt % vs 33 wt %). These results demonstrate that the inclusion of carbon microspheres is an effective way to facilitate the mass transport of air and methanol, emphasizing the importance of pore structure at both the cathode and anode in the development of efficient self-breathing direct methanol fuel cells.

1. Introduction

Fuel cells have attracted great interest as an ideal primary energy conversion device with high-energy conversion efficiency and low pollutant emission. Recently, direct methanol fuel cells (DMFCs) have come into favor because of their low operating temperatures and use of a liquid fuel. In DMFCs, Pt-based alloy catalysts are used for methanol oxidation[1−5] at the anode and oxygen reduction[6−9] at the cathode, but insufficient catalytic activity has challenged the commercial application of DMFCs. Enormous efforts have been made toward the development of new electrocatalysts, with novel synthetic methodologies being employed to improve catalytic performance.[10−16] Electrocatalysts for fuel cells are caught between the demands for high conductivity and high catalyst loading[17−24] (which are best met by nanoparticles of noble metals on nanoparticles of carbon) and the requirement of high mass transport of methanol at the anode and of O_2 at the cathode[17,18,22,24] (which is hindered by the dense packing of carbon nanoparticles).

In general, fuel cell catalysts are prepared as small nanoparticles dispersed on a carbon support to provide better utilization of the expensive noble metals. Carbon blacks, such as Vulcan XC-72 (a registered trade name from CABOT), have been widely used as supports for fuel cell catalysts due to their high conductivities and high surface areas. Recent studies, however, have revealed that the physical properties of the carbon support can greatly affect the electrochemical properties of the fuel cell catalyst.[25−31] It has been reported that carbon materials with both high surface area and good crystallinity can not only provide a high dispersion of Pt nanoparticles, but also facilitate electron transfer, resulting in better device performance.[21,32] In addition, nanoporous carbons with 3D-ordered pore structures have been shown to improve the mass transport of reactants and products during fuel cell operation.[33−35]

Ultrasonic spray pyrolysis (USP) has long been used in industry for the continuous production of ultrafine powders and nanoparticles.[36] New materials prepared by this technique (e.g., porous and nanostructured metal oxides and sulfides, as well as luminescent semiconductor nanoparticles) have been used as catalysts, drug carriers, sensors, and electronic and magnetic materials.[37−42] Very recently, USP has been demonstrated as a facile and novel method for meso- and macroporous carbon powder synthesis.[43] Typically, meso- and macroporous carbons are prepared by tedious templating methods in which crystalline mesoporous silicas or colloidal silica crystals are mixed with a carbon source; the composite is then carbonized.[22,33,44−51] Subsequent chemical leaching with hydrofluoric acid removes the silica and introduces pores into the remaining carbon material. While nanosized silica particles are commercially available in various sizes, it is troublesome to completely remove template silicas and the process itself is time-consuming and

* Corresponding authors. E-mail: ksuslick@uiuc.edu (Suslick); hasuckim@snu.ac.kr (Kim).
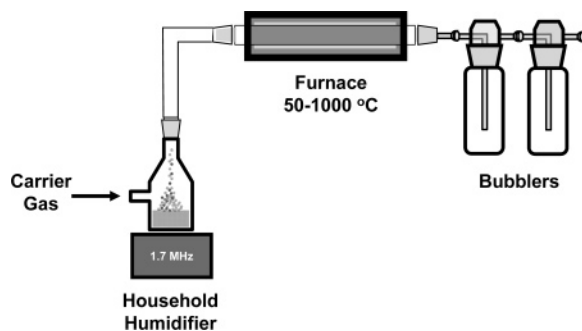† University of Illinois at Urbana-Champaign.
‡ Seoul National University.

Figure 1. Ultrasonic spray pyrolysis (USP) experimental apparatus. A humidifier ultrasonically nebulizes a precursor solution producing a mist of micrometer-sized droplets. The aerosol droplets are then carried by argon gas into a furnace where solvent evaporation and precursor decomposition occur. Bubblers collect the porous carbon, and byproducts remain dissolved in the collection solvent or are flushed out of the system by the carrier gas.

inefficient. With the USP approach, porous carbons with various pore structures can be synthesized simply and continuously without the use of a template. In this study, two of these porous carbons were prepared and evaluated as a new carbon support material for the fuel cell catalyst and as a pore-forming material in a MEA.

2. Experimental Section

Synthesis. A pictorial representation of a laboratory-scale USP setup is shown in Figure 1. A household humidifier operating at 1.7 MHz (Sunbeam model no. 696) nebulizes the precursor solution. The nebulization cell has two inlets, one for the inert gas sweep and the second for the addition of precursor solution; its base is a 52 mm diameter opening with an O-ring groove, over which a polyethylene membrane (2 mils) is clamped, and the cell is then placed directly above the humidifier transducer, which is submerged in water as a coupling medium. The inert gas flow carries the aerosol droplets through a single zone furnace with a total heated region of ~30 cm where precursor decomposition occurs. The product is then collected in a series of four water bubblers attached to the furnace outlet.

The precursors used in this work were a 1.5 M aqueous solution of lithium dichloroacetate or sodium chloroacetate, which generate the porous carbon products denoted PC-I and PC-II, respectively.[43] Prior to synthesis, the solutions were sparged with argon. The pyrolysis of the nebulized mist was conducted in an argon flow (2.0 scfh) with a furnace temperature of 700 °C through a 25 mm quartz tube (total heated region ~30 cm). The powders produced were isolated from the collection media by centrifugation. To remove any residual alkali chloride salt (generated as a byproduct during precursor decomposition), the powder was re-suspended in pure water and isolated again by centrifugation, and the washing procedures were repeated several times. The washed powders were then collected in ethanol, which was easily removed by rotary evaporation to accumulate the powders, which were then dried under vacuum at ~100 °C.

PC-I, PC-II, and Vulcan XC-72 were used as a support for PtRu electrocatalysts. These catalysts were prepared by a surfactant-stabilized colloidal method developed by Bönnemann et al.[52] with some modification. Anhydrous $PtCl_2$ and $RuCl_3$ were dissolved in tetrahydrofuran (THF), and the required amount of a carbon sample was added to the solution and stirred to form a homogeneous slurry. A 1 M (octyl)$_4$N[BEt$_3$H] solution in THF was added dropwise under vigorous stirring. The reaction vessel was then placed in an oil bath at 40 °C overnight.

The material was filtered, rinsed thoroughly with excess ethanol and water several times, and dried under air. Finally, the catalysts were heat-treated at 300 °C in an atmosphere of 10% O_2/N_2 gas mixture for 10 min, then 10% H_2/N_2 for 10 min; this protocol is necessary to remove any residual organic species and fully reduce the catalysts. The metal loading on each carbon was 90 wt %, as confirmed by elemental analysis; the Pt/Ru ratios were taken from the stoichiometry employed during synthesis. The resulting catalysts will hereafter be referred to as PtRu/PC-I, PtRu/PC-II, and PtRu/Vulcan, respectively.

Characterization. Scanning electron microscopy (SEM) images of each carbon were obtained with a Hitachi S-4700, and transmission electron microscopy (TEM) images of the porous carbons and catalysts were taken with JEOL 2010F and Phillips CM12 TEMs. Nitrogen adsorption and desorption isotherms were measured with an ASAP 2010 Micropore System (Micromeritics, USA) at liquid nitrogen temperature (−196 °C), and the specific surface areas were determined according to the Brunauer−Emmett−Teller (BET) method. The pore size distributions of the porous carbons were analyzed using the Barrett−Joyner−Halenda (BJH) method with desorption branches. Powder X-ray diffraction (XRD) patterns of each catalyst were obtained with a M18XHF-SRA diffractometer (MAC Science Co.) using Cu Kα radiation. A CHN analyzer (Flash EA 1112) was used to determine the amount of carbon in the synthesized catalysts. Resistivities of carbon mixtures (PC-I and Vulcan XC-72) were measured using the 4-point probe method with a Keithley Source Meter (model 2400). Particle size distributions of the carbon mixtures were obtained using a particle size analyzer (Multisizer 3, Beckman-Coulter).

Electrochemical Measurements. Electrodes for a DMFC unit cell test were prepared using a spray method. A homogeneous suspension of poly(tetrafluoroethylene) and Acetylene Black Powder (Denka, Japan) was sprayed onto a carbon cloth (E-TEK) to form a gas diffusion layer. Each catalyst was then suspended in a mixture of isopropyl alcohol and Nafion solution (Aldrich, 5 wt % in water/aliphatic alcohols) and stirred to form a homogeneous slurry. The weight ratio of metal to dry Nafion was 10:2. The slurry was sprayed onto the prepared gas diffusion layer. For the fabrication of MEAs with anodes made from a mixture of catalysts (PtRu/PC-I and PtRu/Vulcan), weight ratios of PtRu/Vulcan to PtRu/PC-I were tested at 1:1, 1:2, and 1:3. Cathode electrodes were prepared in the same way using a Pt/C catalyst (E-TEK, 60 wt % Pt) except with a weight ratio of metal to Nafion of 10:5. For the preparation of MEAs with a mixture of Pt/C (E-TEK, 60 wt % Pt) and PC-II on the cathode, the PC-II was added to the Pt/C catalyst in the amounts of 1.25, 2.5, and 5 wt %. The catalyst loading at the anode and cathode were 5 and 3 mg (metal)/cm^2, respectively. The MEAs for a unit cell test were prepared by hot-pressing (135 °C, 100 kgf/cm^3 for 3 min) the anode and cathode layers onto both sides of a pretreated Nafion 117 membrane (Du-Pont). The geometric area of a unit cell was 1 cm^2.

For unit cell operation, an aqueous solution of 2 M methanol was fed to the anode at a rate of 2 cm^3/min. The air for the cathode was pre-humidified at 40 °C and supplied to the cathode at flow rates of either 200 or 1000 cm^3/min. Both reactants were passed through a heated zone maintained at 40 °C. The operation of the unit cell was performed at ambient pressure, and the cell temperature was maintained at 70 °C. The potential−current response of the unit cell was measured galvanostatically with an electronic loader.
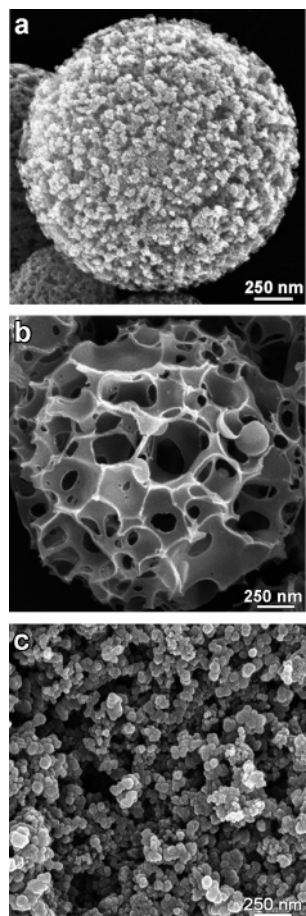
Porous Carbon Supports for DMFC Electrodes

J. Phys. Chem. C, Vol. 111, No. 29, 2007 **10961**

Figure 2. SEM micrographs of (a) PC-I, (b) PC-II, and (c) Vulcan XC-72.

3. Results and Discussion

Catalyst Morphology. Using ultrasonic spray pyrolysis (USP) for the formation of porous carbons can create a variety of carbon morphologies.[43] The relative order of precursor melting and decomposition processes is particularly important. In PC-I (formed from USP of a lithium dichloroacetate solution), interconnected mesopores are observed within the individual carbon spheres, as shown in Figure 2a. While the USP process facilitates spherical particle formation, the internal pore structure is formed during the precursor decomposition. In the case of PC-I, lithium dichloroacetate decomposition generates LiCl, which then acts as a temporary pore template as the carbon network growth occurs;[43] collection of the product and workup in water removes the generated salt and reveals the porous nature of the carbon material. In PC-I, precursor melting comes first, and then decomposition follows;[43] salt formation in PC-I occurs with decarboxylation of the precursor, leading to formation of mesopores in carbon spheres.

In contrast, the internal pore structure of the PC-II particles (formed from USP of a sodium chloroacetate solution) is quite different (Figure 2b). Here, large macropores are present, which generates a much more open carbon network. As with PC-I, the internal pore structure of PC-II is the result of the precursor decomposition pathway and, in this case, the generation of NaCl as a temporary template. In PC-II (unlike PC-I), no melting occurs before precursor decomposition; as a result, the carbon network forms through solid-state reactions, resulting in macropore formation.[43]

Finally, the SEM of the commercially available Vulcan XC-72 (Figure 2c) shows a very different morphology compared to
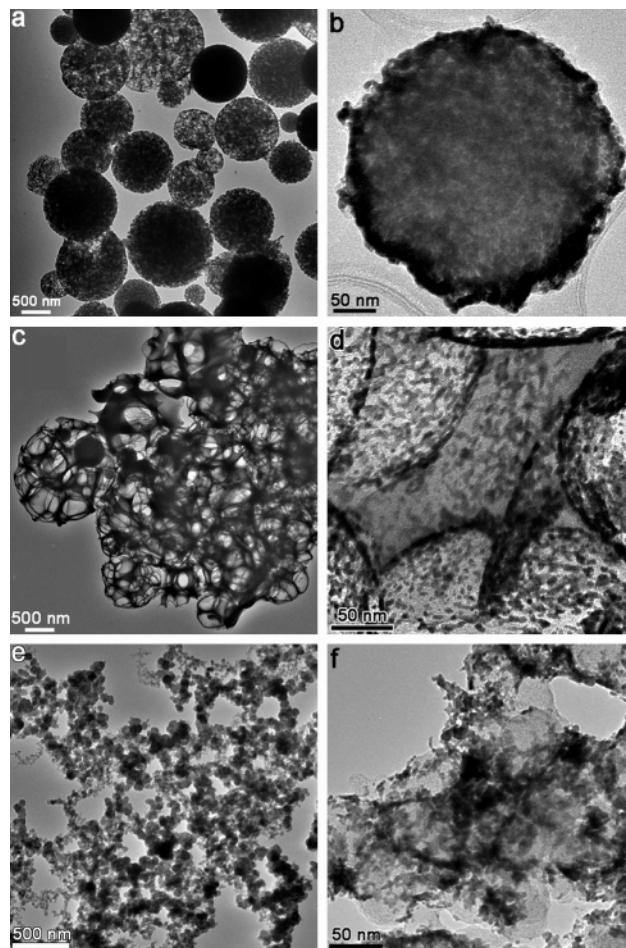

Figure 3. TEM micrographs of carbons and PtRu catalysts supported on each carbon. (a) PC-I, (b) PtRu/PC-I, (c) PC-II, (d) PtRu/PC-II, (e) Vulcan XC-72, and (f) PtRu/Vulcan.

that of the two USP carbons. The Vulcan carbon is composed of nanosized carbon particles, extensively agglomerated, with micropores only.

The pore size distribution and surface area of porous carbons synthesized using USP were probed by nitrogen sorption analysis (Supporting Information). The Brunauer−Emmett−Teller (BET) surface areas of PC-I and PC-II were found to be 718 and 69 m^2/g, respectively, and of Vulcan XC-72, 213 m^2/g. The pore size distributions show that both USP carbons have broad pore size distributions. In PC-I, mesopores ranging from 5 to 50 nm are developed in individual carbon spheres, whereas only macropores are observed in PC-II, consistent with the SEM observations.

Figure 3, parts a and b, shows TEM images of PC-I and 90 wt % PtRu/PC-I, respectively. When 90 wt % metal catalyst is loaded on PC-I, PtRu nanoparticles agglomerate on the surface of PC-I. While PC-I has a relatively large surface area (718 m^2/g), most of its pores are developed inside the carbon spheres, and as a result, the surface area accessible for PtRu nanoparticles is not sufficient enough to achieve good dispersion of the nanoparticles. Figure 3, parts c and d, reveals the morphology of PC-II and 90 wt % PtRu/PC-II, respectively. Again, PC-II and 90 wt % PtRu/PC-II have large macropores, which generate a much more open catalyst structure. Because of the large and open pore structure of PC-II, the PtRu nanoparticles are adsorbed on both the inner and outer walls of PC-II, leading to a good dispersion of nanoparticles throughout the entire carbon network. Figure 3, parts e and f, shows TEM images of Vulcan XC-72 and 90 wt % PtRu/Vulcan, respec-
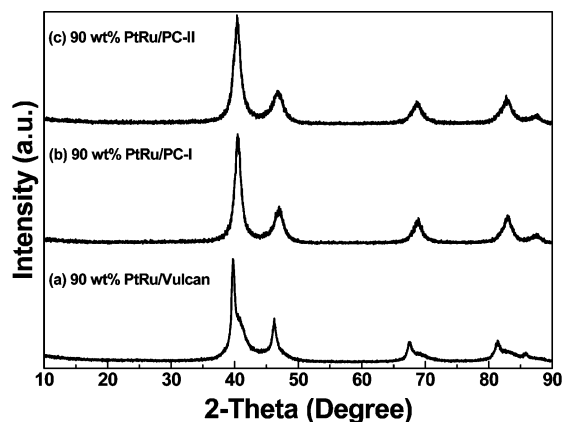
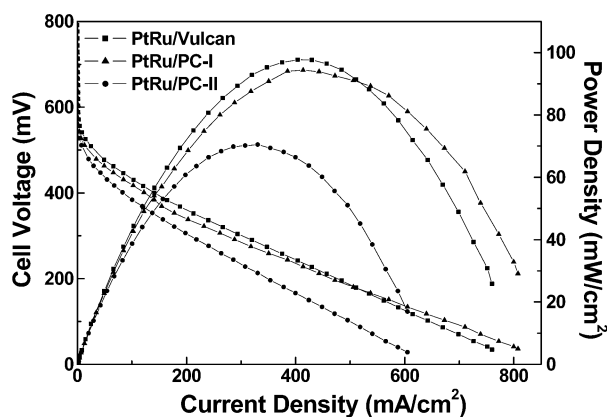**Figure 4.** XRD diffraction patterns of carbon-supported PtRu catalysts.

Figure 5. Voltage and power density responses of carbon-supported PtRu anode catalysts in a direct methanol fuel cell. Unit cell conditions: cell temperature, 70 °C; PtRu anode catalyst loading, 5 mg/cm^3; Pt cathode catalyst loading, 3 mg/cm^3; methanol flow rate, 2 cm^3/min; and airflow rate, 1000 cm^3/min.

tively. For Vulcan XC-72, rounded interconnected carbon particles several tens of nanometers in size are observed. Given the size of the nanoparticles of carbon in Vulcan XC-72, it is not surprising to see extensive agglomeration of PtRu nanoparticles when supported on Vulcan XC-72 (Figure 2c).

Figure 4 gives the XRD patterns of the carbon-supported catalysts. All of the catalysts show a typical face-centered cubic (fcc) Pt lattice and no peaks related to RuO$_2$ or Ru phases are observed, confirming PtRu alloy formation. Alloy formation is also supported by the Pt(111) peak positions which are shifted toward higher 2θ positions as compared to pure Pt (e.g., 39.7645°). The average particle sizes of the three catalysts (PtRu/Vulcan, PtRu/PC-I, and PtRu/PC-II), calculated from the (220) peak using the Debye–Scherrer equation, are 9.7, 6.4, and 5.6 nm, respectively. These are in good agreement with the TEM observations (Supporting Information).

Electrocatalysis at the Anode. Figure 5 shows the unit cell performances of MEAs in a DMFC with either PtRu/PC-I or PtRu/PC-II as the anodic catalyst and compares them to PtRu/Vulcan. The PtRu/PC-II catalyst exhibits lower performance than both PtRu/PC-I and PtRu/Vulcan over the entire current density region. The poor performance seen with PtRu/PC-II is probably due to higher ohmic resistance of the MEA as compared to the other catalysts.

While PtRu/Vulcan shows a slightly higher performance than that of PtRu/PC-I in the activation-controlled region (low current density region), its activity for methanol oxidation in the mass transport-controlled region (high current density region) is lower than that of PtRu/PC-I. PtRu/PC-I also shows lower activity
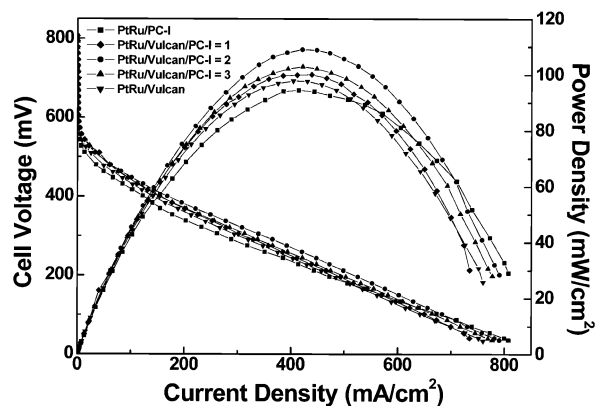

Figure 6. Voltage and power density responses of anode PtRu catalyst mixtures supported on PC-I and Vulcan XC-72, respectively. The unit cell conditions are the same as those in Figure 5.

than PtRu/Vulcan in the low current density region; this is likely due to relatively low connectivity between carbon networks, which leads to poor conductivity. PC-I, however, provides more space in the MEA due to the micrometer-sized spheres, which helps prevent flooding of the electrode caused by water and blocking of the mass transport channels by carbon dioxide bubbles produced during the unit cell operation and results in a better performance in the high current density region.

One would wish to combine the high conductivity of Vulcan XC-72 and the improved mass transport that results from the larger particle size of PC-I. To optimize the internal pore structure of the MEA without loss of conductivity for maximum performance, we examined mixtures of both of these two carbon catalysts (PtRu/PC-I and PtRu/Vulcan) for the MEA fabrication. The voltage and power density responses of the MEAs prepared with the mixed catalysts are given in Figure 6. As shown in Figure 6, the maximum power densities are 94.4, 100.0, 109.0, 102.9, and 93.7 mW/cm^2 for PtRu/PC-I alone, PtRu/Vulcan/PC-I (1:1), PtRu/Vulcan/PC-I (2:1), PtRu/Vulcan/PC-I (3:1), and PtRu/Vulcan alone, respectively. PtRu/Vulcan/PC-I (2:1) exhibits 16% higher power density than the PtRu/Vulcan, as well as a better performance in the high current density region. Thus, for the anodic catalyst, PtRu/Vulcan/PC-I (2:1) represents the optimum compromise between increased Pt utilization and mass transport versus decreased conductivity.

A schematic diagram of the mixed catalyst systems is shown in Figure 7. When PtRu/PC-I is used alone, empty space exists between each carbon sphere in the MEA, which aids in the effective mass transport of the fuel and the product during unit cell operation. Upon adding PtRu/Vulcan to PtRu/PC-I, the poor conductivity of the MEA should be greatly improved, but as the amount of PtRu/ Vulcan dominates, the Vulcan XC-72 carbon nanoparticles begin fill the free space between the PC-I microspheres, blocking the mass-transport channels created by the micrometer-sized PC-I spheres.

The synergic effect proposed in Figure 7 was evaluated by resistivity measurements and particle size distribution analysis of the carbon mixtures (PC-I and Vulcan XC-72). The resistivities of PC-I, Vulcan/PC-I (1:1), Vulcan/PC-I (2:1), Vulcan/PC-I (3:1), and Vulcan are 56.55, 4.31, 3.87, 1.29, and 0.20 Ω cm, respectively. These measurements confirm that PC-I is a poor conductor as compared to Vulcan XC-72, but that indeed we can recover much of the conductivity in the mixed carbon systems. The particle size distributions of the carbon mixtures are shown in Figure 8. PC-I spheres are largely distributed in the 1–2 μm region, which is consistent with TEM observations. Adding more Vulcan XC-72 into the carbon mixture increases
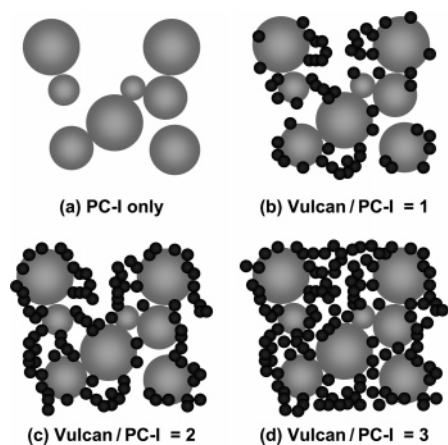
Porous Carbon Supports for DMFC Electrodes

J. Phys. Chem. C, Vol. 111, No. 29, 2007 **10963**

Figure 7. Schematic diagram of catalyst mixtures. By using both carbon microspheres and carbon nanoparticles, one can provide both higher conductivity and more effective diffusion channels for the fuel and its products.
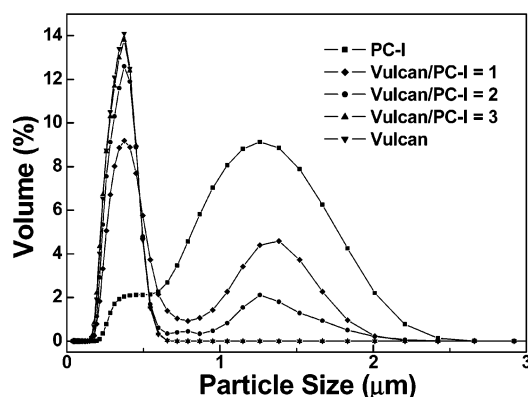

Figure 8. Particle size distributions of carbon mixtures used in the preparation of the anode catalysts.

Figure 9. Voltage and power density responses of cathode catalysts made from Pt/C (60 wt % Pt, E-TEK) mixed with various amounts of PC-II at an airflow rate of (a) 1000 and (b) 200 cm^3/min. Unit cell conditions: cell temperature, 70 °C; PtRu anode catalyst (60 wt % PtRu, E-TEK) loading, 5 mg/cm^3; Pt cathode catalyst loading, 3 mg/cm^3; and methanol flow rate, 2 cm^3/min.

the volume percentage of submicrometer-sized particles but at the expense of the micrometer-sized particle regime. The submicrometer-sized particles can be packed more compactly than the micrometer-sized particles in a MEA, and thus prevent effective diffusion of the reactant and products.

Electrocatalysis at the Cathode. In order to evaluate PC-II as an effective pore former for the cathode, PC-II was mixed at varying ratios with a commercially available Pt/C catalyst (60 wt % Pt, E-TEK) for MEA fabrication. The E-TEK Pt/C catalyst has a morphology very similar to that of Vulcan XC-72, which is not surprising since the E-TEK catalyst is made from Vulcan XC-72 (www.etek-inc.com). Since air, which is usually fed to the cathode in a real DMFC application, includes only 20% of oxygen, the effective diffusion of oxygen at the cathode during the fuel cell operation can be as important as the effective diffusion of methanol at the anode. Figure 9 shows the unit cell performances of the MEAs with differing amounts of PC-II added to the cathode. The highest performance is observed in a MEA with 1.25 wt % PC-II added to the cathode with airflow rates of either 200 or 1000 cm^3/min, with the overall performance gradually decreasing as the amount of PC-II in the cathode was increased. Figure 9 confirms for the cathode the same type of optimization as we saw earlier for the anode; an intermediate amount of PC-II must be used to facilitate oxygen diffusion and improve overall device performance, but above some critical weight percent, further PC-II incorporation inhibits performance. For the cathode, this decrease in current response upon adding more PC-II may also be due to ineffective formation of triple-phase boundaries among metal catalyst,
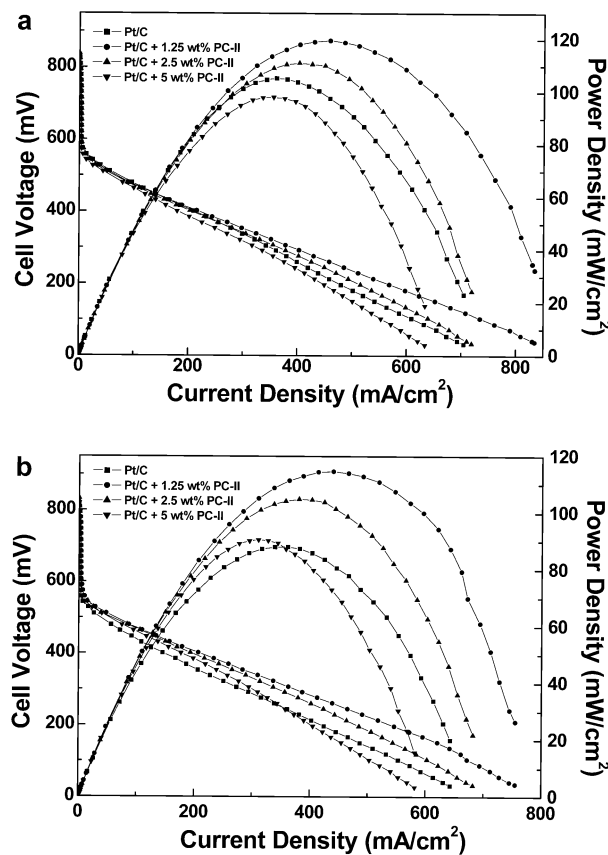
reactants, and Nafion ionomer, which is one of the critical factors for an effective MEA fabrication. The effect of PC-II on the performance appears even more dramatic at a low-airflow rate. As the airflow rate was decreased from 1000 to 200 cm^3/min, the maximum power density in the MEA with 1.25 wt % PC-II added did not change significantly, whereas the MEA prepared without the use of the PC-II showed ~20% decrease in the maximum power density.

4. Conclusions

Electrocatalysts for fuel cells are caught between the demands for high conductivity and high catalyst loading (which are best met by nanoparticles of noble metals on nanoparticles of carbon) and the requirement of high mass transport (of methanol at the anode and of O$_2$ at the cathode). Ultrasonic spray pyrolysis (USP) provides a simple and facile way to prepare porous carbons with various morphologies and pore sizes. In exploring these new morphologies of carbon, two types of porous carbon microspheres were tested as pore-forming additives for both the anode catalyst (i.e., PtRu/C for methanol oxidation) and the cathode catalyst (i.e., Pt/C for O$_2$ reduction). The anode catalyst mixture of PtRu/Vulcan and PtRu/PC-I (weight ratio 2:1, 33 wt % PC-I) showed the highest performance improvement and is attributed to the synergic effect of two carbons (PC-I and Vulcan XC-72); the mixture improves the effective mass transport of reactant methanol and products, while maintaining a reasonably high conductivity. For the reduction of O$_2$ at the cathode, the addition of a relatively small amount of carbon microspheres (PC-II) significantly improved the performance

of the cathode when it was added to the E-TEK commercial Pt/C catalyst. Even at a relatively slow airflow rate, the maximum power density of the membrane electrode assembly with 1.25 wt % PC-II was maintained without a significant decrease. O_2 is, of course, much less viscous than methanol, so the difference in the amount of pore loading required is much less for the cathode than for the anode (i.e., 1.25 wt % vs 33 wt %). These results demonstrate that the inclusion of carbon microspheres is an effective way to facilitate the mass transport of air and methanol, emphasizing the importance of pore structure at both the cathode and anode in the development of efficient self-breathing direct methanol fuel cells.

Supporting Information Available: Pore size distributions and TEM micrographs. This material is available free of charge via the Internet at http://pubs.acs.org.

References and Notes

(1) Lu, A. H.; Schmidt, W.; Spliethoff, B.; Schuth, F. *Adv. Mater.* **2003**, *15*, 1602.

(2) Kua, J.; Goddard, W. A. *J. Am. Chem. Soc.* **1999**, *121*, 10928.

(3) Ley, K. L.; Liu, R. X.; Pu, C.; Fan, Q. B.; Leyarovska, N.; Segre, C.; Smotkin, E. S. *J. Electrochem. Soc.* **1997**, *144*, 1543.

(4) Arico, A. S.; Antonucci, V.; Giordano, N.; Shukla, A. K.; Ravikumar, M. K.; Roy, A.; Barman, S. R.; Sarma, D. D. *J. Power Sources* **1994**, *50*, 295.

(5) Frelink, T.; Visscher, W.; van Veen, J. A. R. *Surf. Sci.* **1995**, *335*, 353.

(6) Li, H. Q.; Xin, Q.; Li, W. Z.; Zhou, Z. H.; Jiang, L. H.; Yang, S. H.; Sun, G. Q. *Chem. Commun.* **2004**, 2776.

(7) Salgado, J. R. C.; Antolini, E.; Gonzalez, E. R. *Appl. Catal., B: Environ.* **2005**, *57*, 283.

(8) Toda, T.; Igarashi, H.; Uchida, H.; Watanabe, M. *J. Electrochem. Soc.* **1999**, *146*, 3750.

(9) Xiong, L.; Manthiram, A. *Electrochim. Acta* **2004**, *49*, 4163.

(10) Bock, C.; Paquet, C.; Couillard, M.; Botton, G. A.; MacDougall, B. R. *J. Am. Chem. Soc.* **2004**, *126*, 8028.

(11) Xue, X.; Lu, T.; Liu, C.; Xing, W. *Chem. Commun.* **2005**, 1601.

(12) Ganesan, R.; Lee, J. S. *Angew. Chem., Int. Ed.* **2005**, *44*, 6557.

(13) Fernandez, J. L.; Raghuveer, V.; Manthiram, A.; Bard, A. J. *J. Am. Chem. Soc.* **2005**, *127*, 13100.

(14) Liao, S.; Holmes, K.-A.; Tsaprailis, H.; Birss, V. I. *J. Am. Chem. Soc.* **2006**, *128*, 3504.

(15) Shao, M.-H.; Sasaki, K.; Adzic, R. R. *J. Am. Chem. Soc.* **2006**, *128*, 3526.

(16) Lee, Y. H.; Lee, G.; Shim, J. H.; Hwang, S.; Kwak, J.; Lee, K.; Song, H.; Park, J. T. *Chem. Mater.* **2006**, *18*, 4209.

(17) Chai, G. S.; Shin, I. S.; Yu, J.-S. *Adv. Mater.* **2004**, *16*, 2057.

(18) Chai, G. S.; Yoon, S. B.; Yu, J.-S.; Choi, J.-H.; Sung, Y.-E. *J. Phys. Chem. B* **2004**, *108*, 7074.

(19) Han, S.; Yun, Y.; Park, K.-W.; Sung, Y.-E.; Hyeon, T. *Adv. Mater.* **2003**, *15*, 1922.

(20) Hyeon, T.; Han, S.; Sung, Y.-E.; Park, K.-W.; Kim, Y.-W. *Angew. Chem., Int. Ed.* **2003**, *42*, 4352.

(21) Park, K. W.; Sung, Y. E.; Han, S.; Yun, Y.; Hyeon, T. *J. Phys. Chem. B* **2004**, *108*, 939.

(22) Yu, J.-S.; Kang, S.; Yoon, S. B.; Chai, G. *J. Am. Chem. Soc.* **2002**, *124*, 9382.

(23) Park, I.-S.; Park, K.-W.; Choi, J.-H.; Park, C. R.; Sung, Y.-E. *Carbon* **2007**, *45*, 28.

(24) Chai, G. S.; Yoon, S. B.; Kim, J. H.; Yu, J.-S. *Chem. Commun.* **2004**, 2766.

(25) Bessel, C. A.; Laubernds, K.; Rodriguez, N. M.; Baker, R. T. K. *J. Phys. Chem. B* **2001**, *105*, 1115.

(26) Steigerwalt, E. S.; Deluga, G. A.; Lukehart, C. M. *J. Phys. Chem. B* **2002**, *106*, 760.

(27) Hull, R. V.; Li, L.; Xing, Y.; Chusuei, C. C. *Chem. Mater.* **2006**, *18*, 1780.

(28) Li, W. Z.; Liang, C. H.; Qiu, J. S.; Zhou, W. J.; Han, H. M.; Wei, Z. B.; Sun, G. Q.; Xin, Q. *Carbon* **2002**, *40*, 791.

(29) Han, K. I.; Lee, J. S.; Park, S. O.; Lee, S. W.; Park, Y. W.; Kim, H. *Electrochim. Acta* **2004**, *50*, 791.

(30) Liu, Y. C.; Qiu, X. P.; Huang, Y. Q.; Zhu, W. T. *Carbon* **2002**, *40*, 2375.

(31) Zhang, W. H.; Shi, J. L.; Wang, L. Z.; Yan, D. S. *Chem. Mater.* **2000**, *12*, 1408.

(32) Takasu, Y.; Kawaguchi, T.; Sugimoto, W.; Murakami, Y. *Electrochim. Acta* **2003**, *48*, 3861.

(33) Joo, S. H.; Choi, S. J.; Oh, I.; Kwak, J.; Liu, Z.; Terasaki, O.; Ryoo, R. *Nature* **2001**, *412*, 169.

(34) Raghuveer, V.; Manthiram, A. *Electrochem. Solid-State Lett.* **2004**, *7*, A336.

(35) Su, F. B.; Zeng, J. H.; Bao, X. Y.; Yu, Y. S.; Lee, J. Y.; Zhao, X. S. *Chem. Mater.* **2005**, *17*, 3960.

(36) Kodas, T. T.; Hampden-Smith, M. *Aerosol Processing of Materials*; Wiley-VCH: New York, 1999.

(37) Patil, P. S. *Mater. Chem. Phys.* **1999**, *59*, 185.

(38) Okuyama, K.; Lenggoro, W. *Chem. Eng. Sci.* **2003**, *58*, 537.

(39) Xia, B.; Lenggoro, W.; Okuyama, K. *Adv. Mater.* **2001**, *13*, 1579.

(40) Skrabalak, S. E.; Suslick, K. S. *J. Am. Chem. Soc.* **2005**, *127*, 9990.

(41) Suh, W. H.; Suslick, K. S. *J. Am. Chem. Soc.* **2005**, *127*, 12007.

(42) Didenko, Y.; Suslick, K. S. *J. Am. Chem. Soc.* **2005**, *127*, 12196.

(43) Skrabalak, S. E.; Suslick, K. S. *J. Am. Chem. Soc.* **2006**, *128*, 12642.

(44) Jun, S.; Joo, S. H.; Ryoo, R.; Kruk, M.; Jaroniec, M.; Liu, Z.; Ohsuna, T.; Terasaki, O. *J. Am. Chem. Soc.* **2000**, *122*, 10712.

(45) Lee, J.; Sohn, K.; Hyeon, T. *J. Am. Chem. Soc.* **2001**, *123*, 5146.

(46) Jang, J.; Lim, B. *Adv. Mater.* **2002**, *14*, 1390.

(47) Lee, J.-S.; Joo, S. H.; Ryoo, R. *J. Am. Chem. Soc.* **2002**, *124*, 1156.

(48) Jang, J.; Lim, B.; Choi, M. *Chem. Commun.* **2005**, 4214.

(49) Sayari, A.; Yang, Y. *Chem. Mater.* **2005**, *17*, 6108.

(50) Yoon, S. B.; Chai, G. S.; Kang, S. K.; Yu, J.-S.; Gierszal, K. P.; Jaroniec, M. *J. Am. Chem. Soc.* **2005**, *127*, 4188.

(51) Gierszal, K. P.; Jaroniec, M. *J. Am. Chem. Soc.* **2006**, *128*, 10026.

(52) Bönnemann, H.; Braun, G.; Brijoux, W.; Brinkmann, R.; Tilling, A. S.; Seevogel, K.; Siepen, K. *J. Organomet. Chem.* **1996**, *520*, 143.